Applied Water Science (2022) 12:249
https://doi.org/10.1007/s13201-022-01779-0

ORIGINAL ARTICLE

Design and direct preparation of a novel silicon carbide support for zeolite membrane

Gangling Chen[1] · Jianying Zhang[1] · Miaomiao Geng[1] · Jaka Sunarso[2] · Ngie Hing Wong[2] · Tianlin Ma[1] · Yujie Wang[1] · Guihua Chen[3]

Received: 20 July 2022 / Accepted: 29 September 2022 / Published online: 10 October 2022

Abstract

The support for the membrane is the basis for the preparation and application of the zeolite membrane. Moreover, its cost and properties directly determine the performance of the zeolite membrane and its industrial applications. A novel porous silicon carbide (SiC) support for zeolite membrane bonded with needle-like mullite ($3Al_2O_3{\cdot}2SiO_2$) was prepared using SiC powders as the raw material and kaolin, $Al(OH)_3$, and AlF_3 as the needle-like mullite precursor additives via an in situ high-temperature reactions in an air atmosphere. Effects of the support material composition and the sintering temperature on the sintering behavior, pore structure, permeability, and microstructure of the resultant supports were extensively investigated. The needle-like mullite formation consumed silicon oxide (SiO_2) and generated a rigid skeleton structure with a good pore structure and bonding phase. Hence, the porous SiC support exhibited high porosity, with relatively large pore size and mechanical strength, which helped improve the support performance. Notably, the porous SiC support sintered at 1480 °C with in situ inter-particle needle-like mullite bonding exhibited excellent filtration and permeability performance. The porous support materials and methods used in this work are suitable for designing and preparing a novel porous SiC support for zeolite membranes.

Keywords Needle-like mullite · Silicon carbide · Zeolite membrane support

Introduction

Zeolites have magnificent prospects with their unique advantages in separation and purification technology and membrane reactor applications. Hence, zeolites have become popular research material for inorganic membranes (Gao et al. 2021; Chen et al. 2021; Wang et al. 2019; Park et al. 2017). Many years ago, Mitsui (Japan) shipbuilder introduced the zeolite NaA membrane to industrial applications (Morigami et al. 2001). However, the high demand for its raw and support materials for membrane synthesis has led to its high production cost, thus limiting its expansion and application. Moreover, the selection and preparation of the support material for the zeolite membrane and their research findings directly affect the development and application of the membrane technology (Zhu et al. 2021; Liang et al. 2021; Cho et al. 2010; Caro et al. 2000; Li et al. 2013; Huang et al. 2013; Shao et al. 2014; Das et al. 2010; Sato and Nakane 2007). Hence, to obtain adequate and efficient zeolite membranes, the support materials for the zeolite membranes, including their material properties and microstructure characteristics, must be designed and appropriately synthesized (Zhu et al. 2021; Sato and Nakane 2007; Lik et al. 2000; Chen et al. 2022; Maarten Biesheuvel and Verweij 1999; Liu et al. 2021).

Although silicon carbide (SiC) shares some characteristics with ceramic oxide materials, its uniqueness lies in high corrosion and heat shock resistance and almost zero

✉ Gangling Chen
chengangd@126.com

✉ Ngie Hing Wong
nhwong@swinburne.edu.my

[1] School of Material Science and Chemical Engineering, Chuzhou University, 239000 Chuzhou, People's Republic of China

[2] Research Centre for Sustainable Technologies, Faculty of Engineering, Computing and Science, Swinburne University of Technology, Jalan Simpang Tiga, 93350 Kuching, Sarawak, Malaysia

[3] School of Pharmaceutical and Material Engineering, Taizhou University, 318000 Jiaojiang, People's Republic of China

water wetting angle (Liu et al. 2021; Xu et al. 2021; Jiang et al. 2021). Such excellent hydrophilic property highlights the potential of using SiC porous material as a zeolite NaA membrane support, which can significantly improve the dehydration efficiency and reduce the handling product costs, especially for the dehydration process of industrial solvent. However, as a covalent compound, SiC generally requires a higher than 2000 °C sintering temperature, thus increasing the material manufacturing costs. Studies have attempted to lower the SiC sintering temperature and preparation costs. Dey et al. 2013 adopted a preparation method that depends on the base reaction process to generate silicon dioxide (SiO_2) as the binder phase, thus reducing the sintering temperature to 1300 °C.

Nevertheless, the thermal expansion of SiO_2 is more significant than that of SiC. In other words, the membrane support prepared using SiO_2 as the binder phase has lower mechanical properties and thermal shock resistance. Besides, the existence of SiO_2 can weaken the corrosion resistance to alkali during the hydrothermal synthesis of the alkali zeolite membrane. Hence, SiO_2 cannot meet the requirements as the support materials for the zeolite membranes. In contrast, mullite ($3Al_2O_3.2SiO_2$) has a lower thermal expansion similar to SiC, which translates to a lower sintering temperature and excellent acid resistance (Schneider et al. 2008; Chen et al. 2015; Wong et al. 2001; Kazemimoghadam et al. 2004; Asghari et al. 2008). Notably, mullite has an elementary composition close to that of zeolite NaA, which may suppress the ionic diffusion and reaction between support and membrane materials during the synthesis of the zeolite membrane. Hence, mullite has recently been studied as the primary support material for zeolite membrane application (Chen et al. 2015; Wong et al. 2001).

Unfortunately, as a porous material, the presence of excessive pores in support can lower its mechanical property. One of the effective ways to toughen and reinforce ceramic materials is using whiskers (Asghari et al. 2008; Guo et al. 2012; Colombo 2008). Currently, there are two main methods to improve the mechanical strength of ceramic materials, i.e., through external introduction or base generation (Colombo 2008). For example, whiskers can be prepared and introduced to the base materials externally. However, it is difficult to sinter the materials and disperse the whiskers effectively without introducing defects and/or poor spray deposition and uniformity (Chen et al. 2015, 2008). Such a problem is less likely to occur if whiskers are prepared through base generation by adding the raw materials under high temperature to the basal body, leading to better mechanical strength.

Mullite whiskers with needle-like structures have been reported to provide stable pore structure, thus enhancing the penetrating quality of cellular material due to the rigid skeleton provided by the whisker (Asghari et al. 2008; Guo et al. 2012; Colombo 2008; Chen et al. 2008). When a mullite precursor is added to the SiC, the needle-like structure can be generated in situ. Although this can be an ideal method for preparing a highly porous SiC support with excellent mechanical properties as the membrane support, there are only a few related studies. Besides, to our best knowledge, a base-generated binder phase with a needle-like mullite whisker is yet to be developed and characterized as SiC support for the zeolite membrane.

In this work, we developed a novel porous SiC support for zeolite membranes via the sintering reaction using SiC powder as the aggregate, and the added kaolin, aluminum fluoride, and aluminum hydroxide as the material of needle-like-structured mullite precursor. We systematically investigated the effects of several process parameters on the microstructure, pore structure, and penetrating and mechanical properties. We also explored the formation mechanism of the porous SiC support for zeolite membranes.

Experimental

Materials and sample preparation

Silicon carbide (SiC) particle (D_{50} = 8 μm, Hebei Tenai Welding Material Co., Ltd., China) and high-purity kaolin ($Al_2O_3{\cdot}2SiO_2{\cdot}2H_2O$, #1000 Mesh, China Kaolin Clay Co., Ltd) and aluminum hydroxide ($Al(OH)_3$, industrial-grade with 65 wt.% alumina content), aluminum fluoride (AlF_3, Shanghai Aladdin Biochemical Technology Co., Ltd, China) were prepared as the primary starting materials. Two starting powders were prepared: SiC and SiC + $Al_2O_3{\cdot}2SiO_2{\cdot}2H_2O$ + $Al(OH)_3$, denoted as S and SM, respectively. The pure SiC was used to form the green body directly. The SM was doped with 5 wt% AlF_3. Here, we briefly described the preparation procedures: (a) add 85% high-purity SiC (with 5 wt.% AlF_3) directly to the 15% kaolin and $Al(OH)_3$ mixture (with 65 wt.% alumina), (b) grind the mixtures of the starting powders, (c) add a certain amount of binder and lubricant after adequate mixing, (d) condense the mixture on the powder crystal tablet machine, with the fake body sized of φ 30 × 2 mm and the strip body sized of 50 × 6 × 6 mm (769YP-24B, Tianjin Keqi Hign & New Technology Cooperation, China), (e) dry the sample in an oven at 110 °C for 5 h, (f) sinter the prepared support material in the specified air atmosphere temperature from 1330 to 1530 °C for 2 h with the heating rate of 3 °C min^{-1} using a programmable electric stove (PD-MJ17, Luoyang Pengda electric furnace factory, China), and lastly (g) cool the product gradually to room temperature.

Characterization

A scanning electron microscope equipped with an energy-dispersive X-ray spectroscopy (SEM–EDX, FEI Quanta200, Netherlands) was used to observe the morphology and chemical composition of the samples. The phase composition of the samples prepared at different sintering temperatures was analyzed by a powder X-ray diffractometer (XRD, D8 advance, Bruker Instrument Co., Ltd., Germany) with the 2θ range of 10-80°. The samples' average pore size was determined using the gas bubble pressure method, following the American Society for Testing and Materials (ASTM) Publication (F316–80). We also measured the sample's porosity according to the Archimedean method (GB1996-80) with water as the liquid medium, as briefly described here: (a) weigh the prepared sample (dry weight) and record it as m_o, (b) mix it with deionized water and boil the mixture for 2 h, (c) weigh the sample again in the water and air, and record them as m_1 and m_2, respectively, and (d) calculate the porosity using Eq. (1). Moreover, we also characterized the samples (support materials) for their bending (mechanical) strength. We used a universal test machine (CMT6203, Shenzhen Reger Instrument Co., Ltd., China) according to the three-point bending method with a 40 mm supporting point span and 0.5 mm min^{-1} loading rate.

$$P = \frac{m_2 - m_0}{m_2 - m_1} \tag{1}$$

Filtration and permeability tests

Figure 1 shows the schematic diagram of the experimental cross-flow filtration setup for testing the filtration and permeability performance of the support sample using deionized water as the medium. Here, we briefly described the testing procedures: (a) operate the pressure difference for the filter between 0.1 and 0.3 MPa, (b) obtain three groups of data for each operating pressure, (c) calculate the average flow rate for each corresponding pressure, (d) determine the filtration and permeability performance of the porous samples using Eq. (2) (Lukasiewicz and Reed 1988; Reed 1993), where Q is the volume flow rate of deionized water, P is the operative pressure, η is the viscosity of deionized water, L is the sample thickness, and A_{eff} is the effective filtration membrane area of the sample, (e) calculate the volume fraction of the sample's pore structure based on the open-pore and closed-pore using Eq. (3), where r is the average pore size of the sample; the open-pore structure can be sub-divided into the structure with one end closed and the structure with both ends open and connected; the structure with both ends open and connected plays a role during the filtration process of porous materials and lastly (f) calculate the fraction of penetrating porosity for open-pore using Eq. (4), where ε_o is the sample's open-porosity measured by Archimedean method.

$$K_P = \frac{\mathrm{d}Q}{\mathrm{d}P}\frac{\eta L}{A_{\text{eff}} r^2} \tag{2}$$

$$\varepsilon_{\text{eff}} = 24\frac{\mathrm{d}Q}{\mathrm{d}P}\frac{\eta L}{A_{\text{eff}} r^2} \tag{3}$$

$$\tau = \frac{\varepsilon_{\text{eff}}}{\varepsilon_o} \times 100\% \tag{4}$$

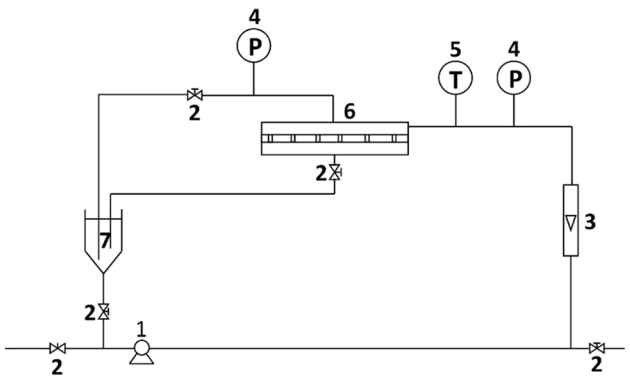

Fig. 1 Schematic diagram of cross-flow filtration experimental equipment [1—Centrifugal pump; 2—Valves; 3—Rotameter; 4—Pressure gauges; 5—Temperature gauge; 6—Ceramic membrane module plate; 7—Feed tank]

Results and discussion

Characterization

Figure 2 shows the SEM images of the two raw material samples (SM and S) sintered at 1480 °C in an air atmosphere for 2 h. We noticed that distinct needle-like particles formed their connections among the silicon carbide (SiC) particles (Fig. 2a). At the same time, the net-like structures also appeared in the sample (Fig. 2b). They were interwoven with the produced needle-like particles, which could still provide sufficient porosity and enhance the penetrating quality. Moreover, the analysis of the chemical composition of the needle-like particles prepared with the SM raw materials indicates 9.38, 42.04, 27.85, and 0.73 wt.% of C, O, Al, and Si, respectively. This result, especially for the Al and Si contents, confirms the presence of mullite ($3Al_2O_3{\cdot}2SiO_2$) as the support material by meeting its stoichiometric composition. Unlike the SM sample, the SiC particles piled up together after the sintering reaction in the S sample (Fig. 2c). We also noticed that the silicon dioxide (SiO_2) generated from the

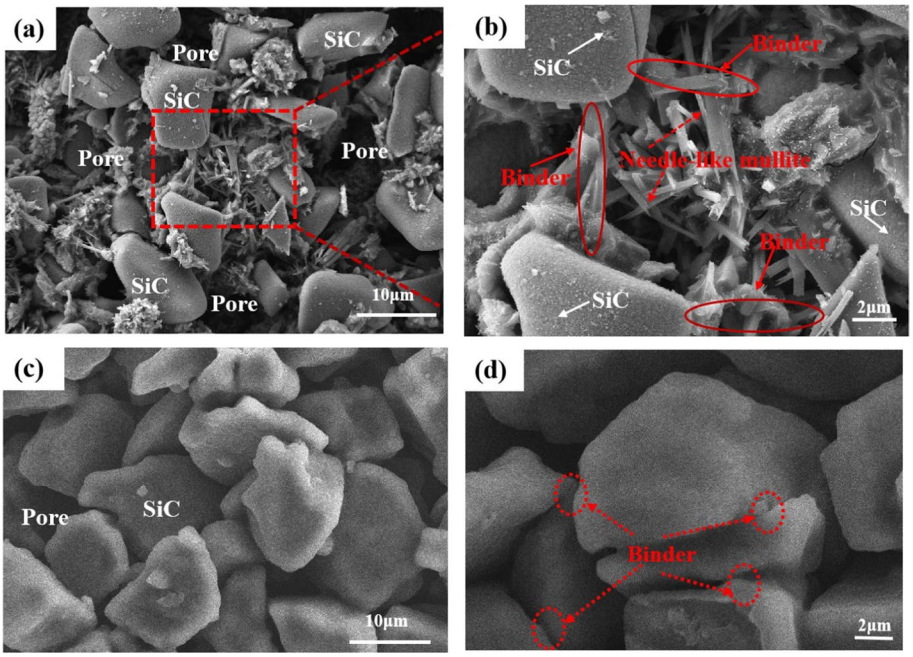

Fig. 2 SEM images of the prepared (**a**–**b**) SM and (**c**–**d**) S samples sintered at 1480 °C in an air atmosphere for 2 h

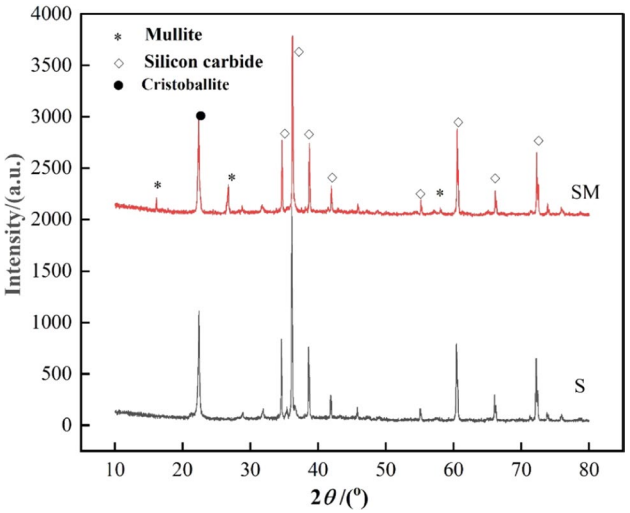

Fig. 3 Powder XRD patterns of the S and SM samples sintered at 1480 °C in an air atmosphere for 2 h

oxidized SiC at high temperatures managed to connect the SiC particles through pore-to-pore contact (Fig. 2d). At the same time, this oxidation reaction yielded mellow and full SiC particles that piled up the pore structure in the sample.

Figure 3 displays the powder XRD patterns of the prepared S and SM samples sintered at 1480 °C in an air atmosphere for 2 h. We noticed that the distinct diffraction peaks of the S sample indicate the presence of SiC composition only, i.e., without mullite ($3Al_2O_3{\cdot}2SiO_2$) and cristobalite (SiO_2). Unlike the S sample, the different diffraction peaks of the SM sample indicate it comprised mostly the SiC binder and some mullite ($3Al_2O_3{\cdot}2SiO_2$) but only a bit of cristobalite (SiO_2) when we added the needle-like mullite precursor to the SM sample. The weaker intensity for cristobalite (SiO_2) characteristic peaks can be ascribed to the base-generated reaction at a high sintering temperature between the needle-like mullite precursor and the generated SiO_2 from the oxidized SiC to form the mullite ($3Al_2O_3{\cdot}2SiO_2$). The results also demonstrate that the needle-like particles formed among the SiC particles had yielded the mullite phase for the sample. As a result, the production of the needle-like mullite phase significantly decreased the SiO_2 content in the SiC sample under the high-temperature oxidation in the air atmosphere.

Sintering mechanism

Figure 4 shows the powder XRD patterns of the prepared samples using the needle-like mullite precursor sintered at 1330, 1380, 1430, 1480, and 1530 °C in an air atmosphere for 2 h. This analysis was carried out to gain insights into the sintering mechanism. Based on the diffraction patterns, the mullite ($3Al_2O_3{\cdot}2SiO_2$) and cristobalite (SiO_2) phases appear at 2θ of 16°, 27°, 66°, and 22°, respectively, after sintering at 1330 °C. However, the characteristic peak of the cristobalite phase at $2\theta$of 22° grows more substantially at 1480 °C than at the other temperatures. This result suggests that the content of the cristobalite phase gradually increases with increasing sintering temperature in the samples below 1480 °C. This can be ascribed to the gradual transformation of amorphous SiO_2 formed through the accelerated oxidation on the SiC surface (Eq. (5)) into the cristobalite phase

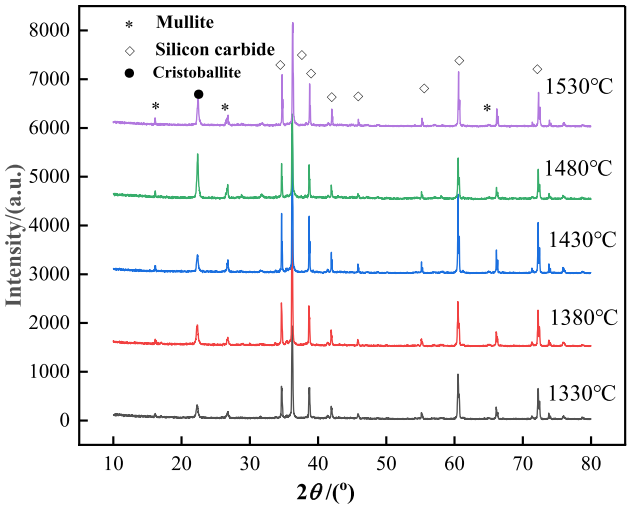

Fig. 4 Powder XRD patterns of the different specimens sintered at 1330, 1380, 1430, 1480, and 1530 °C in an air atmosphere for 2 h

with increasing sintering temperature. When the sintering temperature reaches 1530 °C, the diffraction peak of the cristobalite phase in the sample weakens. This may be due to its transformation to the glass phase at a high sintering temperature, which contributed to the formation of the mullite phase.

Similarly, the mullite phase's diffraction peaks at 2θ of 16°, 27°, and 66° also intensify with increasing sintering temperature. This phenomenon can be ascribed to the generation of topaz (Eqs. (6–9)) with the addition of the needle-like mullite precursor. After that, the topaz continuously reacted (Eq. (11)) with the SiO_2 generated from the oxidized SiC (Eq. (5)) and produced more mullite (Eq. (11)). Lastly, the final phase composition of the sample was mainly affected by the sintering temperature (Fig. 4). Mullite continuously formed the mullite phase in the sample made at a higher sintering temperature. Hence, the diffraction peak of the mullite phase also intensifies. Figure 5 illustrates a schematic diagram of the sintering process of needle-like mullite-bonded SiC support using the needle-like mullite precursor.

$$SiC + 2O_2 \rightarrow SiO_2 + CO_2 \tag{5}$$

$$Al_2O_3 \cdot 2SiO_2 \cdot 2H_2O\ (\text{kaolin}) \xrightarrow{400-500^\circ C} Al_2O_3 \cdot 2SiO_2 + 2H_2O \tag{6}$$

$$2\left(Al_2O_3 \cdot 2SiO_2\right) \xrightarrow{\sim 950^\circ C} Si_3Al_4O_{12} + SiO_2 \tag{7}$$

$$3Si_3Al_4O_{12} \xrightarrow{\rangle 1050^\circ C} 2\left(3Al_2O_3 \cdot 2SiO_2\right)(\text{mullite}) + 5SiO_2 \tag{8}$$

$$2AlF_3 + 2SiO_2 \xrightarrow{800-950^\circ C} Al_2\left(SiO_4\right)F_2(\text{topaz}) + SiF_4 \tag{9}$$

$$3SiF_4 + 2Al_2O_3 \rightarrow 4AlF_3 + 3SiO_2 \tag{10}$$

$$6Al_2\left(SiO_4\right)F_2 + SiO_2 \rightarrow 2\left(3Al_2O_3 \cdot 2SiO_2\right)(\text{mullite}) + 3SiF_4 \tag{11}$$

On the one hand, needle-like mullite consumed the SiO_2 from the oxidized SiC under high temperature. It simultaneously established a rigid skeleton structure with the mullite network that connected aggregates by point-to-point contact, providing novel porous support for zeolite membranes with high porosity and relatively large pore size. As a result, the amount of SiO_2 gradually decreased in the sample while the amount of needle-like mullite formed in the bonded phase gradually increased. Hence, the SiO_2 residues after the reaction were extremely low. Moreover, because SiO_2 was prone to react with alkali, reducing its content could substantially improve the alkali resistance of the sample. Hence, the sintering process significantly enhanced the strength of particle boundary, which promoted the sample's mechanical strength and chemical stability.

On the other hand, kaolin ($Al_2O_3{\cdot}2SiO_2{\cdot}2H_2O$) mainly experienced thermal treatment reactions during the heating

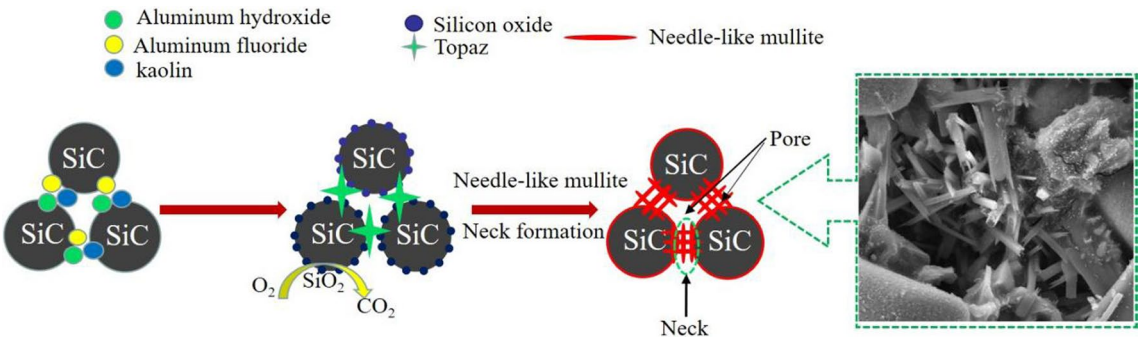

Fig. 5 A schematic showing the sintering process of needle-like mullite-bonded SiC support

process in accordance with Eqs. (6–8) (Eom et al. 2009). Studies suggested that the following main reactions occurred during the preparation of needle-like mullite-bonded SiC support (Haught and Talmy 1990a, 1990b): (a) SiF_4 generated in Eq. (9) reacted with Al_2O_3 in the powder material to generate AlF_3 and SiO_2 (Eq. (10)), (b) AlF_3, SiO_2, and Al_2O_3 in the raw material reacted until they were transformed into topaz (Eqs. (9) and (10)), (c) when the temperature continued rising to 1200 °C, more SiO_2 were generated in the sample due to the accelerated oxidation on the SiC surface (Eq. (5)), (d) at this moment, the topaz generated in the previous step began to react with SiO_2 to generate more needle-like mullite (Eq. (11)) and simultaneously consumed the SiO_2 generated from the oxidized SiC surface (Eq. (5)).

Porosity and pore structure

Figure 6 shows the porosity of the prepared S and SM samples sintered at various temperatures in an air atmosphere for 2 h. The porosities of both S and SM samples decreased with increasing sintering temperature. However, the porosity of the SM sample prepared using needle-like mullite precursor was significantly higher than that of the S sample prepared solely using SiC. The S sample's porosity decreased from 36.3% at 1330 °C to 30.6% at 1530 °C. This result can be ascribed to the SiC surface continued to oxidize, forming the SiO_2 glass phase, thus increasing the sintering degree among particles with increasing sintering temperature.

Similarly, the SM sample's porosity decreased from 43.8% at 1330 °C to 37.2% at 1530 °C. By adding $Al(OH)_3$ to the SM sample, the aluminum piled up at SiC particles. However, it began to decompose and formed pores during the heating at high temperature, thus increasing the porosity of the support sample. However, the reduction in porosity for the SM support sample (with needle-like mullite precursor) was slower than that of the S support sample (without needle-like mullite precursor) when the sintering temperature was above 1380 °C. Such phenomenon can be ascribed to the generated SiO_2 from the oxidized SiC reacted with Al_2O_3 (Eqs. (6–11)) at a higher temperature (above 1380 °C) and simultaneously generated needle-like mullite (Fig. 4). Moreover, the melting point of mullite was higher than that of SiO_2. The viscosity of mullite was lower at high temperature (Eom et al. 2009).

Figure 7 shows the average pore size of the prepared S and SM samples sintered at various temperatures in an air atmosphere for 2 h. The average pore size of SM sample (with needle-like mullite precursor) increased gradually from 1.01 μm at 1330 °C to 1.32 μm at 1480 °C with increasing sintering temperature. However, its average pore size decreased to 1.23 μm when the sintering temperature rose to 1530 °C. This result is because the in situ reaction among SiC ceramic particles gradually occurred, generated needle-like mullite, and formed the neck connection with increasing sintering temperature due to the addition of needle-like mullite precursor (Fig. 5). Due to the growth of mullite crystal, the pores among SiC particles were enlarged, which resulted in the formation of large pores and the disappearance of small ones, thus increasing the pore size to a certain extent (Chen et al. 2008). However, an excessive amount of the silica glass phase could form due to the rapid oxidation on the SiC surface when the sintering temperature exceeds a certain value. This amorphous glass phase can diffuse into the pores of the support sample, thus decreasing the porosity and pore size of the support sample. On the other hand, the S sample's surface with only SiC was oxidized to generate

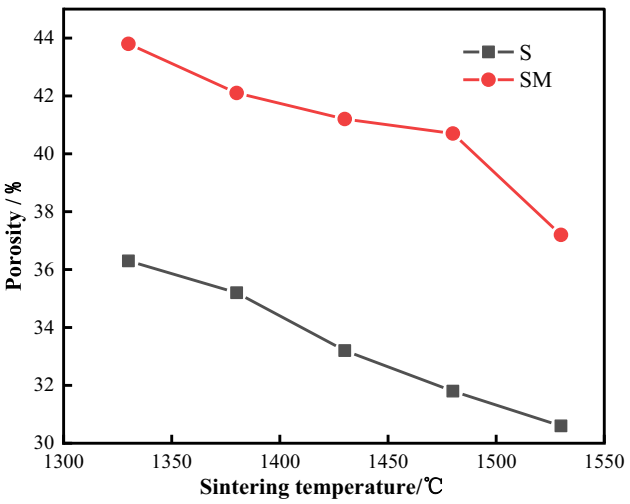

Fig. 6 The porosity of the support samples sintered at various temperatures in an air atmosphere for 2 h

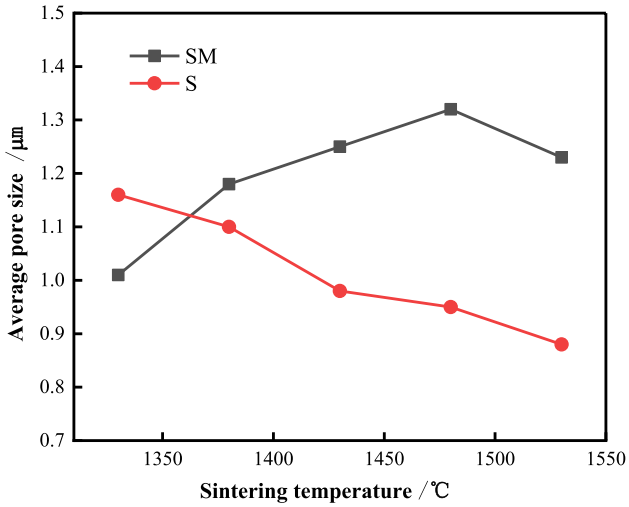

Fig. 7 The average pore size of the support samples sintered at various temperatures in an air atmosphere for 2 h

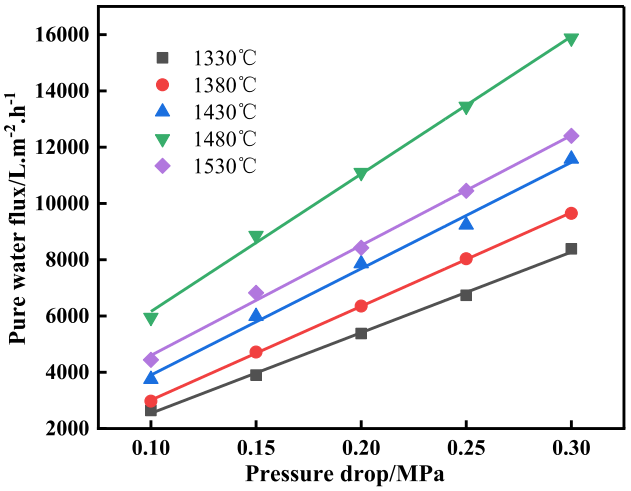

Fig. 8 Pure water flux with the pressure drop results from the cross-filtration test for the support samples SM prepared at different sintering temperatures

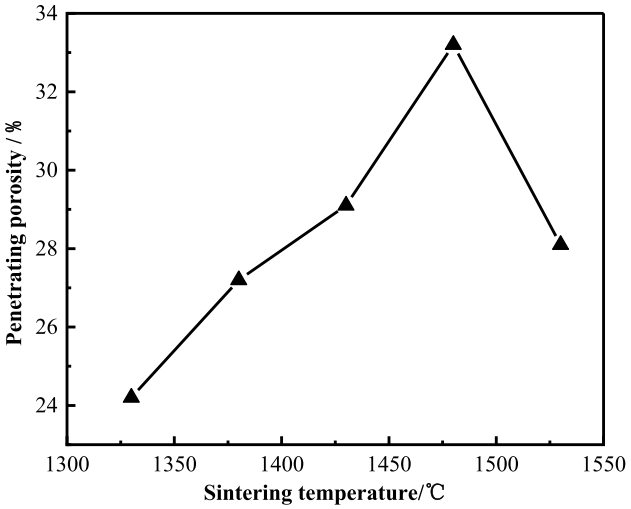

Fig. 9 Penetrating porosity of support samples SM sintered at various temperatures in an air atmosphere for 2 h

a SiO_2 glass phase, demonstrating densifying behavior as the sintering temperature increased. Hence, its pore size decreased as the sintering temperature increased.

Filtration and permeability performance

Figure 8 shows the pure water flux as a function of pressure drop from the cross-filtration test for the support samples (SM) prepared at different sintering temperatures. All the samples exhibited increasing water flux with increasing pressure drops and sintering temperature. The only exception to increasing water flux with sintering temperature rise is the sample sintered at 1480 °C. The sample sintered at 1480 °C displayed the highest water flux with the highest pressure drop (gradient) from 6,000 to 16,000 L m^{-2} h^{-1} and 0.10 to 0.30 MPa, respectively. Such trend aligns well with Darcy's law, where the water discharge rate is proportional to the pressure gradient (Lukasiewicz and Reed 1988). Moreover, these results are consistent with the change in pore structure within the sample at this sintering temperature, i.e., the largest average pore size for the SM sample sintered at 1480 °C (Fig. 7).

Figure 9 shows the penetrating porosity of the prepared support samples SM at different sintering temperatures calculated using Eq. (4). Interestingly, the same SM sample sintered at 1480 °C exhibited a maximum penetrating porosity of 33.2%. According to Eq. (4), the penetrating porosity of the SM sample at this sintering temperature accounts for 81.5% of the total open porosity. This result can be ascribed to the fact that mullite had yet to form with needle-like mullite precursor in the sample during the initial sintering stage. At this stage, the partial oxidation on the SiC surface produced the amorphous glass phase, thus increasing its viscous flow with increasing sintering temperature. With temperature rise, $Al(OH)_3$ decomposed into aluminum oxide and acted as a pore-forming agent. Furthermore, the aluminum oxide particles filled inside the pores as the sintering temperature increased. Then, the SiC particles were fused into the glass phase at a high temperature, producing needle-like mullite via the in situ reaction. Lastly, the pore structure became opened among the particles in the sample and formed a penetrating structure, thus enlarging the open porosity and enhancing the sample's permeability performance.

Three-point flexural strength

Figure 10 shows the three-point flexural strength of the support samples at different sintering temperatures. The mechanical strength of the samples increased as the sintering temperature rose from 1330 to 1530 °C. When the sintering temperature was above 1,430 °C, the mechanical strength of the SM sample increased significantly from 23.2 to 37.4 MPa. This phenomenon is most likely due to the in situ reaction between aluminum oxide in the sample and SiO_2 from the oxidized SiC surface at this temperature range, thus reducing the glass phase content and rapidly increasing the mullite phase content in the sample. However, the three-point flexural strength of the support made up of pure SiC sintered at 1330 °C for 2 h was only 7.8 MPa. As the sintering temperature rose to 1530 °C in 2 h, its three-point flexural strength increased to 21.2 MPa. The flexural strength of the S sample did not significantly increase throughout the temperature range. This is because the strength of the S sample was mainly determined by the degree of sintering between particles. The SiC surface continuously oxidized

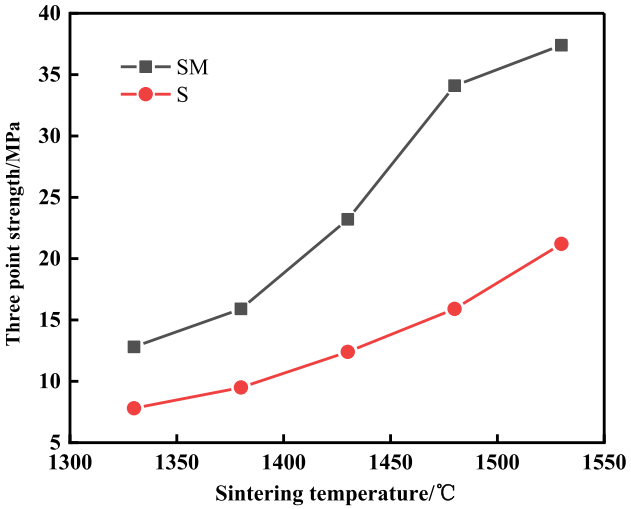

Fig. 10 Three-point flexural strength of the samples sintered at different sintering temperatures

with increasing sintering temperature to form the SiO_2 glass phase, and the sintering degree among SiC particles intensified.

Conclusion

A porous silicon carbide (SiC) support for zeolite membrane bonded with needle-like mullite ($3Al_2O_3{\cdot}2SiO_2$) was prepared via an in situ reaction at high temperature in an air atmosphere using SiC powder as the raw material and needle-like mullite precursor as the additive. Effects of sintering temperature on the formation of porous SiC support microstructure were examined systematically. Then, the formation mechanism of needle-like mullite bonding as a binding phase was explored. We observed that the formation of needle-like mullite managed to consume silicon oxide (SiO_2) formed by high-temperature oxidation of SiC. This process generated needle-like mullite with a rigid skeleton structure. Hence, the porous SiC support exhibited good pore structure and bonding phase with high porosity, relatively large pore size, mechanical strength, and resilience, which helped improve the porous SiC support performance.

The porous SiC support for zeolite membrane prepared through this method with the bonding phase of needle-like mullite was adopted to establish a network structure. This network structure enabled connections with point-to-point contact of aggregates, significantly intensifying the particle boundary. Hence, the sample's mechanical strength and chemical stability were enhanced significantly. The porous SiC support sintered at 1480 °C displayed excellent permeability performance with in situ needle-like mullite inter-particle bonding. At 1480 °C, the porous SiC support achieved 40.7% porosity with 1.32 μm average pore size and 34.1 MPa flexural strength. Consequently, the porous support materials and method used in this work are applicable to make a novel porous SiC support for zeolite membrane.

Acknowledgements The authors gratefully acknowledge funding supports from the University Natural Science Research Major Project of Anhui Province (No. KJ2019ZD043, KJ2020A0707), Anhui Provincial Science and Technology Key R&D Program (No. 2022a05020055), Anhui Provincial Natural Science Foundation (No. 2108085QB53)

Author contributions Gangling Chena contributed to the conceptual study, research idea, and design and wrote the manuscript; Jianying Zhang and Miaomiao Geng performed the experiments; Jaka Sunarso and Ngie Hing Wong helped perform the analysis with constructive discussion; Tianlin Ma, Yujie Wang, and Guihua Chen contributed to analysis and manuscript preparation.

Funding This research received no specific grant from any funding agency in the public, commercial, or not-for-profit sectors.

Declarations

Conflict of interest All authors certify that they have no affiliations with or involvement in any organization or entity with any financial or non-financial interest in the subject matter or materials discussed in this paper.

Ethical approval This article does not contain any studies with human participants or animals performed by any authors.

References

Asghari M, Mohammadi T, Aziznia A, Danayi MR, Moosavi SH, Alamdari RF, Agand F (2008) Preparation and characterization of a thin continuous faujasite membrane on tubular porous mullite support. Desalination 220:65–71

Caro J, Noack M, Kölsch P, Schäfer R (2000) Zeolite membranes—state of their development and perspective. Microporous Mesoporous Mater 38:3–24

Chen G, Qi H, Xing W, Xu N (2008) Direct preparation of macroporous mullite supports for membranes by in situ reaction sintering. J Membr Sci 318:38–44

Chen G, Ge X, Wang Y, Xing W, Guo Y (2015) Design and preparation of high permeability porous mullite support for membranes by in-situ reaction. Ceram Int 41(7):8282–8287

Chen G, Zhang J, Ma T, Wang Y, Chen G, Guo Y (2021) Novel preparation of low-cost support for NaA zeolite membrane by utilizing natural clay. Appl Water Sci 11:160

Chen G, Zhang J, Zhou A, Feng J, Shao X, Ma T, Guo Y (2022) A novel preparation of high permeation SiC supports for NaA zeolite membrane by in situ reaction bonding. Appl Water Sci 12(80):1–8

Cho CH, Oh KY, Yeo JG, Kim SK, Lee YM (2010) Synthesis, ethanol dehydration and thermal stability of NaA zeolite/alumina composite membranes with narrow non-zeolitic pores and thin intermediate layer. J Membr Sci 364:138–148

Colombo P (2008) In praise of pores. Science 322:381–383

Das N, Kundu D, Chatterjee M (2010) The effect of intermediate layer on synthesis and gas permeation properties of NaA zeolite membrane. J Coat Technol Res 7(3):383–390

Dey A, Kayal N, Chakrabarti O, Innocentini MDM, Chacon WS, Coury JR (2013) Evaluation of air permeation behavior of porous SiC ceramics synthesized by oxidation-bonding technique. Int J Appl Ceram Technol 10:1023–1033

Eom JH, Kim YW, Woo SK, Han IS (2009) Effect of submicron silicon carbide powder addition on the processing and strength of reaction-sintered mullite-silicon carbide composites. J Ceram Soc Jpn 117(4):421–425

Gao X, Da C, Chen C, Li Z, Gu X, Bhatia SK (2021) The induced orientation effect of linear gases during transport in a NaA zeolite membrane modified by alkali lignin. J Membr Sci 620:118971

Guo A, Liu J, Wang Y, Xu H (2012) Preparation of porous lamellar mullite ceramics with whisker skeletons by electrospinning and pressure molding. Mater Lett 74:107–110

Haught DA, Talmy IG (1990a) Preparation of Mullite Whiskers from Al_2O_3, SiO_2 and AlF_3 Powders. US Pat. No. 4910172

Haught DA, Talmy IG (1990b) Preparation of Mullite Whiskers. US. Pat. No. 4911902

Huang A, Liu Q, Wang N, Tong X, Huang B, Wang M, Caro J (2013) Covalent synthesis of dense zeolite LTA membranes on various 3-chloropropyltrimethoxysilane functionalized supports. J Membr Sci 437:57–64

Jiang Q, Xie Y, Ji L, Zhong Z, Xing W (2021) Low-temperature sintering of a porous SiC ceramic filter using water glass and zirconia as sintering aids. Ceram Int 47:26125–26133

Kazemimoghadam M, Pak A, Mohammadi T (2004) Dehydration of water/1-1-dimethylhydrazine mixtures by zeolite membranes. Microporous Mesoporous Mater 70:127–134

Li H, Wang J, Xu J, Meng X, Xu B, Yang J, Li S, Lu J, Zhang Y, He X, Yin D (2013) Synthesis of zeolite NaA membranes with high performance and high reproducibility on coarse macroporous supports. J Membr Sci 444:513–522

Liang D, Huang J, Zhang H, Fu H, Zhang Y, Chen H (2021) Influencing factors on the performance of tubular ceramic membrane supports prepared by extrusion. Ceram Int 47:10464–10477

Lik HCJ, Tellez C, Yeung KL, Ho K (2000) The role of surface chemistry in zeolite membrane formation. J Membr Sci 164:257–275

Liu D, Li Y, Lv C, Chen J, Zhang D, Wu Z, Ding D, Xiao G (2021) Permeating behaviour of porous SiC ceramics fabricated with different SiC particle sizes. Ceram Int 47:5610–5616

Lukasiewicz SJ, Reed JS (1988) Specific permeability of porous compacts as described by a capillary model. J Am Ceram Soc 71:1008–1014

Maarten Biesheuvel P, Verweij H (1999) Design of ceramic membrane supports: permeability, tensile strength and stress. J Membr Sci 156:141–152

Morigami Y, Kondo M, Abe J, Kita H, Okamoto K (2001) The first large-scale pervaporation plant using tubular-type module with zeolite NaA membrane. Sep Purif Technol 25:251–260

Park HB, Kamcev J, Robeson LM, Elimelech M, Freeman BD (2017) Maximizing the right stuff: the trade-off between membrane permeability and selectivity. Science 356(6343):1138–1148

Reed JS (1993) Liquid permeability of packed particles: Why perpetuate the carmen-kozeny model? J Am Ceram Soc 76:547–548

Sato K, Nakane T (2007) A high reproducible fabrication method for industrial production of high flux NaA zeolite membrane. J Membr Sci 301:151–161

Schneider H, Schreuer J, Hildmann B (2008) Structure and properties of mullite—A review. J Eur Ceram Soc 28:329–344

Shao J, Zhan Z, Li J, Wang Z, Li K, Yan Y (2014) Zeolite NaA membranes supported on alumina hollow fibers: effect of support resistances on pervaporation performance. J Membr Sci 451:10–17

Wang B, Zheng Y, Zhang J, Zhang W, Zhang F, Xing W, Zhou R (2019) Separation of light gas mixtures using zeolite SSZ-13 membranes. Microporous Mesoporous Mater 275:191–199

Wong WC, Au LTY, Ariso CT, Yeung KL (2001) Effects of synthesis parameters on the zeolite membrane growth. J Membr Sci 191:143–163

Xu X, Liu X, Wu J, Zhang C, Tian K, Yu J (2021) Effect of preparation conditions on gas permeability parameters of porous SiC ceramics. J Eur Ceram Soc 41:3252–3263

Zhu W, Liu Y, Guan K, Peng C, Wu J (2021) Design and optimization of ceramic membrane structure: from the perspective of flux matching between support and membrane. Ceram Int 47:12357–12365